IEEE Access
Multidisciplinary ⋮ Rapid Review ⋮ Open Access Journal

Received 8 November 2022, accepted 20 November 2022, date of publication 23 November 2022,
date of current version 30 November 2022.

Digital Object Identifier 10.1109/ACCESS.2022.3224148

RESEARCH ARTICLE

Bandwidth-Enhanced Compact Circularly-Polarized Wearable Antenna With a Magneto-Electric Dipole

TU TUAN LE, YONG-DEOK KIM, AND TAE-YEOUL YUN, (Member, IEEE)
Department of Electronic Engineering, Hanyang University, Seoul 133-791, South Korea
Corresponding author: Tae-Yeoul Yun (taeyeoul@hanyang.ac.kr)

This work was supported by the National Research Foundation of Korea under Grant 2018R1A5A7025522.

ABSTRACT A compact broadband circularly-polarized wearable antenna is presented for wireless body area network (WBAN) off-body communications. The proposed antenna comprises two substrates, a semi-rigid substrate with low loss-tangent and a textile substrate, that can boost the antenna performance while maintaining wearer comfort. Initially, a crossed-dipole as a fundamental radiator that radiates a circularly polarized (CP) wave is printed on the semi-rigid substrate. A pair of L-shaped slits are loaded into crossed-dipole arm, which significantly miniaturizes the antenna size. A magneto-electric dipole as a parasitic element is loaded to widen axial ratio bandwidth (ARBW) and impedance bandwidth (IBW). A conductive textile is attached to the textile substrate as the ground plane to minimize the specific absorption rate (SAR). The simulated SAR at 5.85 GHz is below the US and EU limit standards. The proposed antenna has solved typical issues in wearable antenna design such as low gain, low radiation efficiency, large size, and narrow IBW and ARBW, while still providing comfortability to wearers.

INDEX TERMS Crossed-dipole, magneto-electric dipole, SAR, WBAN, wearable antenna.

I. INTRODUCTION

In the past decade, studies on body-centric wireless devices have significantly increased. Numerous body-centric devices are expected to be an integral part of the internet of things (IoT) and to be widely used in healthcare, security, and safety [1]. In these applications, a wearable antenna that contributes to the overall efficiency of a wireless link is an essential component in wireless body area network (WBAN) communications. A wearable antenna should be lightweight, flexible, compact, and have high gain and high efficiency. In addition, energy radiating from the wearable antenna to the human body should be minimized to keep the specific absorption rate (SAR) below the international standard.

Although both linearly-polarized (LP) antennas [2], [3], [4], [5], [6], [7], [8], [9], [10], [11], [12], [13] and circularly-polarized (CP) antennas [14, [15], [16], [17], [18], [19] are proposed in WBAN applications, CP antennas are preferred. The CP antenna can ensure the stability of the wireless communication link because it is robust to polarization mismatch and thus provides more accurate data transmission, especially when the position of wearable devices is continuously changing because of the movement of the human body. Several approaches have been proposed to achieve CP radiation in the literature. In [14], an all-textile based antenna adopted a coplanar waveguide (CPW) L-shaped feed line to produce x and y components of the magnetic current for CP waves. A fully flexible CP antenna fabricated by silver nanowires is presented in [15]. CP radiation is enabled by placing a planar LP loop monopole above an artificial ground plane. Another approach implementing a button antenna has some advantages over traditional textile-based antennas [16], [17]. The button antenna allows for a higher profile antenna and it uses a common rigid or semi-rigid substrate that can boost the radiation performance of the antenna compared with the textile-based antenna. However, the abovementioned antennas have relatively narrow axial ratio bandwidths (ARBW); these should be wide enough to overcome the proximity

The associate editor coordinating the review of this manuscript and approving it for publication was Giorgio Montisci.

effect, bending, or movement of human body. To tackle this issue, [18] presents a microstrip patch antenna loaded with a modified metasurface array which produces broadband ARBW. However, this design has a relatively large footprint. An interesting method in [19] presents a compact monopole antenna that uses a jeans textile as a substrate covering ultra-wideband (UWB) application. However, one inherent drawback of the textile substrate is its high loss tangent, which degrades the antenna performance.

In 2006, K. M. Luk, et al. invented a new kind of complementary antenna called the magneto-electric (ME) dipole [20] by combining the electric (E) and magnetic (M) dipoles in one antenna structure. Various studies have adopted a ME dipole [21], [22], [23], [24], [25], [26] that can enhance the antenna bandwidth and radiation performance. Nevertheless, there is limited research on ME dipoles in wearable applications, with the exception of [27]. This antenna is designed based on the conventional magneto-electric dipole topology by combining a planar magnetic dipole (slot antenna) with an electric dipole in a felt substrate. Two U-shaped slots are cut in the electric dipole. As a result, the antenna achieves a wide bandwidth and high radiation performance; however, it generates a LP radiation wave. In order to generate high-gain and high-efficiency while maintaining comfort for wearers, we have proposed the method [3], [28] that combines rigid substrate with low loss-tangent and textile substrate in wearable antenna design. Besides, antenna miniaturization is also a hot topic in wearable antenna design. A wearable antenna should have compact size in order to easily integrate into a garment. Its compactness also helps to reduce the bending effect when the antenna is to be worn. Adopting a slit [2] into the antenna structure introduces additional inductive and capacitive characteristics and significantly reduces the antenna size.

In this paper, we propose a compact broadband CP wearable antenna for WBAN off-body communications. The CP radiation, high gain, and high efficiency are achieved by loaded ME dipole with a compact crossed-dipole antenna. The miniaturization of the proposed antenna is implemented using a pair of L-shaped slits on crossed-dipole arms. Then, a ME dipole is loaded as a parasitic element to significantly enhance impedance bandwidth (IBW) and ARBW. The proposed antenna comprises two substrates: a semi-flexible substrate and a textile substrate. The main radiator is printed on the semi-flexible substrate. A conductive textile layer is adhered to the textile substrate. The proposed antenna has resolved several issues in wearable antenna design including low gain, low radiation efficiency, large size, and narrow IBW and ARBW, while still providing comfortability to wearers. The proposed antenna is verified by deformations of the structure and measurements in both free space and phantom body to show its suitability for off-body communication. The remaining sections of this paper are organized as follows. Section II presents antenna geometry and design, operating mechanism, and deformation study. In Section III, antenna performance in free space and phantom body are investigated. SAR evaluation is also included in this section. The conclusion is given in Section IV.

II. ANTENNA DESIGN AND OPERATING MECHANISM

A. ANTENNA GEOMETRY

The antenna geometry is designed and simulated by ANSYS HFSS v.16. The perspective view, top view, and side view of the proposed antenna are shown in Fig. 1. The antenna comprises two structures: a semi-flexible substrate for the main radiator and a felt textile substrate for the ground plane. The crossed-dipole radiator and the ME dipole as the main radiator are printed on a Rogers 5880 substrate with a relative dielectric constant of 2.2, a loss tangent of 0.0009, a height of 0.508 mm, and a width (W_s) of 23 mm.

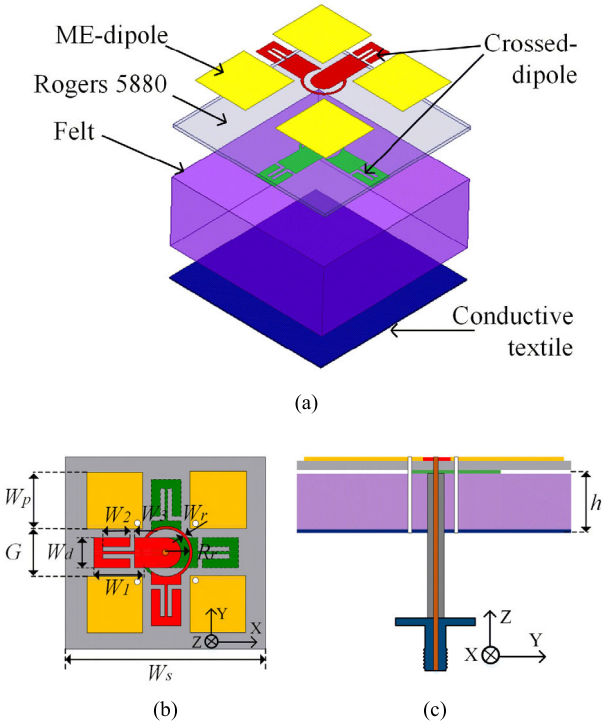

FIGURE 1. Geometry of the proposed antenna in: (a) perspective view, (b) top view, and (c) side view.

The crossed-dipole is designed on both sides of the semi-flexible substrate while the ME dipole is designed on the top side. The crossed-dipole arms are formed by a rectangular strip-line with length and width of W_1 and W_d, respectively. Two L-shaped slits are etched along the edge of the rectangular strip-line to miniaturize the antenna size by lengthening the current path. The length (W_2) and width (W_3) of the slit are shown in Fig. 1 (b). The crossed-dipole arm is connected by a vacant-quarter ring and fed by a 50 Ω coaxial cable. The vacant square-ring acts as a phase delay line that can produce a phase difference of 90° among the crossed-bowtie dipole arms to achieve CP radiation. The upper-half and bottom-half dipoles are connected to the inner and outer axes of the SMA cable, respectively.

The ME dipole consists of four square patch units with the patch length of W_p and four via holes. Each pair of patches can be considered as a planar E dipole [26]. The via hole with a length of h is connected to the ground plane to form the vertical quarter wavelength antenna radiating through the aperture between the patches, which is considered the M-dipole. A felt substrate is placed beneath the semi-rigid substrate. The felt substrate has a relative dielectric constant of 1.4, a loss tangent of 0.044, a height (h) of 8 mm, and a width (W_s). The ground plane is made of a Shieldit^{TM} super conductive textile [29] with a conductivity of 118,000 S/m that is adhered to the backside of the felt substrate. The flexible ground plane greatly reduces SAR and provides comfort to the wearer.

The optimized geometrical parameters are: $W_1 = 7.6$, $W_2 = 2.5$, $W_3 = 0.5$, $W_r = 0.3$, $R_r = 2.6$, $W_d = 3.3$, $W_p = 8$, $G = 4.3$, $W_s = 23$, and $h = 8$ (unit: mm).

B. OPERATING MECHANISM

To understand the operating mechanism of the proposed antenna, the design evoluation is presented in Fig. 2, including a conventional crossed-dipole antenna denoted as Ant1, a proposed antenna without ME denoted as Ant2, and the proposed antenna. For fair comparison, the dimensions of Ant1 and Ant2 are kept the same as the proposed antenna. The comparison with regards to S11, axial ratio (AR), amplitude ratio ($|E_x|/|E_y|$), and phase difference ($\angle E_x - \angle E_y$) are investigated in Fig. 3.

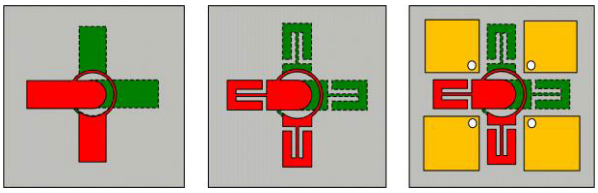

FIGURE 2. Design evolution: (a) Ant1, (b) Ant2, and (c) the proposed antenna.

As shown in Fig. 3 (a), the conventional crossed-dipole Ant1 has poor impedance matching at a targeting resonant frequency of 5.8 GHz. In addition, the amplitude ratio ($|E_x|/|E_y|$) and phase difference ($\angle E_x - \angle E_y$) are greater than 0 dB and 90° at 5.8 GHz, respectively, as shown in Fig. 3 (b) and (c). Therefore, Ant1 radiates a fundamental mode having LP waves with an AR greater than 6 dB, as shown in Fig. 3 (d). By introducing an L-shaped slit pair in the crossed-dipole arm, Ant2 increases the electric current path and shifts the resonant mode to lower frequency. Ant2 has two resonant modes at 5.3 and 6.1 GHz. The amplitude ratio ($|E_x|/|E_y|$) and phase difference are 0 dB and 90° at 5.7 GHz, respectively. A narrow ARBW of 7.7% (5.48–5.92 GHz) is achieved, as shown in Fig. 3 (d). To further improve the antenna performance, Ant2 is loaded with the ME dipole to produce the proposed antenna, as shown

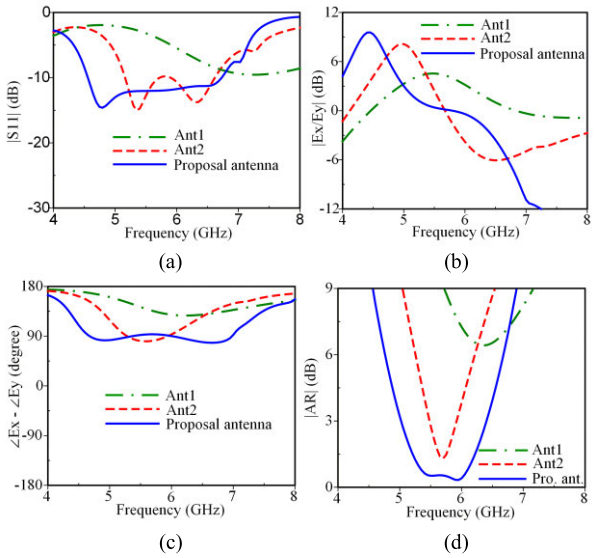

FIGURE 3. Simulated results of three cases: (a) S11, (b) AR, (c) |Ex/Ey|, and (d) ∠Ex − ∠Ey.

in Fig. 2 (c). The ME dipole works as a parasitic radiator exciting an adjacent mode combining with fundamental modes, which significantly increases IBW up to 38.73% (4.56–6.75 GHz) as shown in Fig. 3 (a). A 0 dB amplitude ratio ($|E_x|/|E_y|$) and 90° phase difference are observed over a wide frequency range. In Fig. 3 (d), an adjacent AR mode is excited at lower frequency resulting in broadband ARBW of 24.17% (5.02–6.4 GHz).

To investigate the CP mechanism of the proposed antenna, electric current distributions on the crossed-dipole and patch and magnetic current distributions on apertures between patches at 5.85 GHz are shown in Figs. 4 and 5, respectively. The simulation is performed at two instances of t = 0 and t = T/4, where T is the period of time. J_{es} and J_{ms} are the vector summations of the electric and magnetic current densities, respectively. As shown in Fig. 4, the E-dipole, J_{e1} and J_{e2}, is observed on the crossed-dipole and a pair of the patch, accumulating in J_{es}. As shown in Fig. 5, the M-dipole is also observed at the aperture between the patches, accumulating in J_{ms}. z_{es} and J_{ms} which are excited simultaneously and are orthogonal to each other. In addition, the E-dipole, J_{es}, at t = 0 and t = T/4 are orthogonal and equal in magnitude. A similar observation is found for the M-dipole, where J_{ms} at t = 0 and t = T/4 are orthogonal and equal in magnitude. Both J_{es} and J_{ms} rotate counter-clockwise with time, which produces right-hand circular polarization (RHCP) in the $+z$ direction.

C. PARAMETRIC STUDY

To further understand how antenna parameters affect antenna performance including IBW and ARBW, the parametric study is performed. In this section, effects of key parameters like crossed-dipole length (W_1), slit length (W_2), and parasitic-dipole length (W_p) are studied. When one parameter

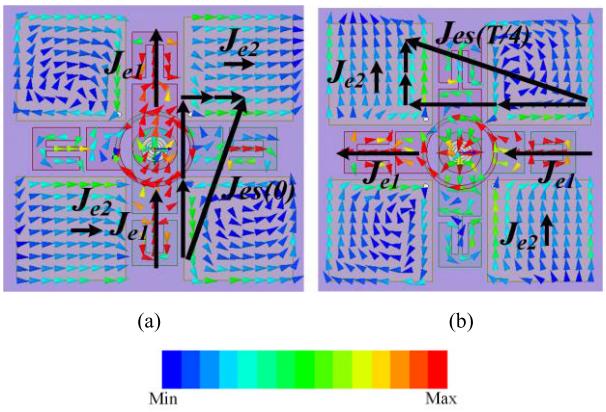

FIGURE 4. Electric current distributions on the crossed-dipole radiator and ME-dipole patch at (a) t = 0 and t = T/4.

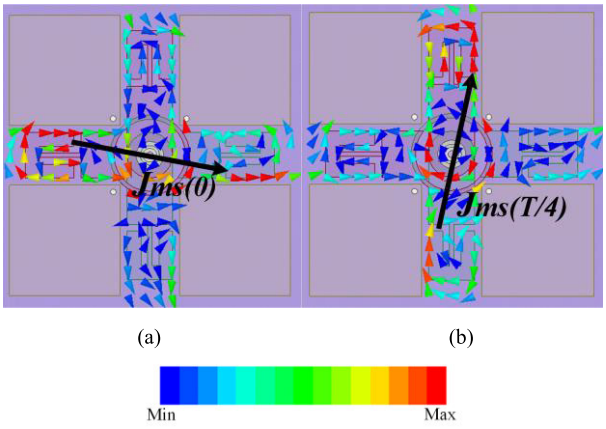

FIGURE 5. Magnetic current distributions on the radiating aperture between the patches at (a) t = 0 and t = T/4.

is under consideration, the others remain at their optimized values.

The parametric study of the crossed-dipole length, W_1, on antenna performance is plotted in Fig. 6. Increasing W_1 increases the current path on the dipole shifting the S11 curve to lower frequency. In addition, varying W_1 strongly affects AR at higher frequency.

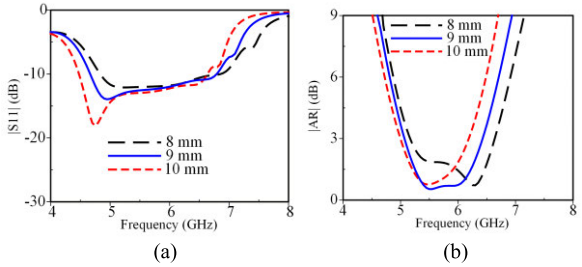

FIGURE 6. Simulated effects of varying dipole length, W_1, on antenna performance: (a) S11 and (b) axial ratio.

The variation of slit length, W_2, on the antenna performance is shown in Fig. 7. The slit length has a strong effect

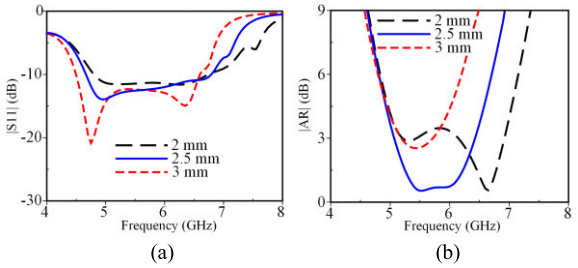

FIGURE 7. Simulated effects of varying slit length, W_2, on antenna performance: (a) S11 and (b) axial ratio.

on both IBW and ARBW. Increasing W_2 makes the surface current path longer on the crossed-dipole shifting the S11 curve to lower frequency. Varying W_2 significantly affects AR at higher frequency. The parametric study of crossed-dipole length, W_1, and slit length, W_2, proves that the crossed-dipole has a strong impact on AR at higher frequency.

The parametric study of the ME-dipole patch length, W_p, on the antenna performance is shown in Fig. 8. Varying W_p has a slight effect on IBW but a strong effect on AR at lower frequency. Increasing W_p lengthens the current path on the parasitic-dipole shifting the AR curve to lower frequency, which proves the parasitic ME-dipole patch has a strong impact on AR at lower frequency.

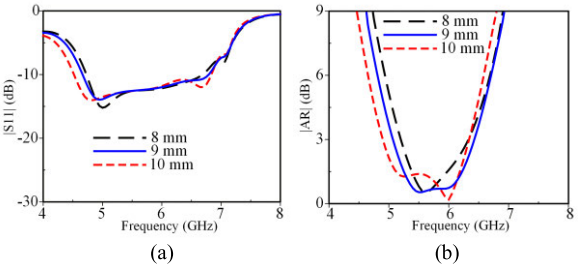

FIGURE 8. Simulated effects of varying parasitic-dipole length, W_p, on antenna performance: (a) S11 and (b) axial ratio.

D. DEFORMATION STUDY

The antenna performance under bending conditions is investigated in this section to show the ability of the proposed antenna when working on an uneven surface. Due to the symmetric geometry of the proposed antenna, only bending in the x-direction is simulated.

The simulated S11 and AR of the proposed antenna bending along a cylinder with a radius of 30, 40, and 50 mm in the x-direction are shown in Fig. 9. As a result of bending the antenna, S11 moves downward or to wider impedance matching. Meanwhile, AR is somewhat diminished. It is noted that frequency shift to higher frequency region is observed for both AR and S11. In addition, S11 and AR bandwidth still cover WBAN applications for all bending radii. Small frequency variation for different bending radius is observed,

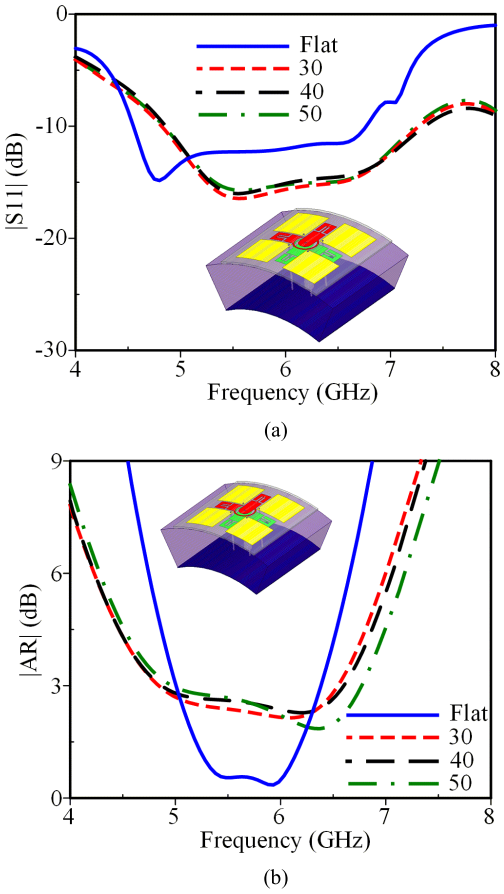

FIGURE 9. Bending effect of the annular-ring radiator in the x-direction: (a) S11 and (b) AR.

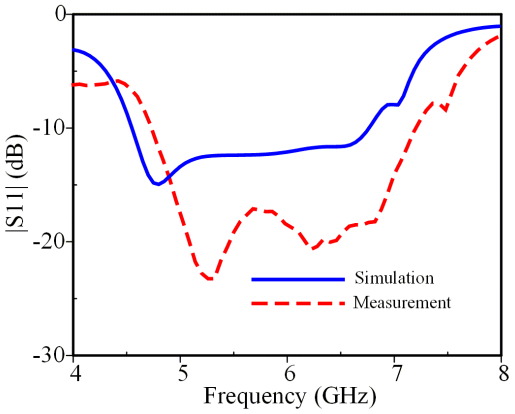

FIGURE 10. Measured S11 in free space.

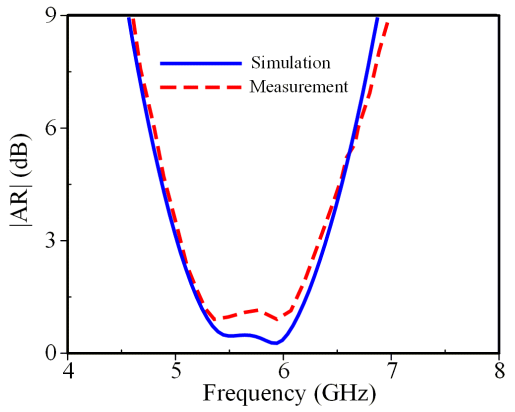

FIGURE 11. Measured AR in free space.

which proves the stable performance of the wearable antenna under bending conditions.

III. ANTENNA PERFORMANCE

In order to verify the simulated results, the proposed antenna is fabricated and then measured in free space and phantom body environments.

A. FREE SPACE PERFORMANCE

Figs. 10 and 11 show the simulated and measured S11 and ARBW in free space. The measured IBW is 40.87% (4.75–7.19 GHz), compared with the simulated result of 38.73% (4.56–6.75 GHz), as shown in Fig. 10. There is somewhat different between simulated and measured data. The discrepancy is caused by the assembled 8-mm felt-substrate that is fabricated from stacking various thin-layer felt substrates and adhering them with acrylic glue, resulting in increased total height of the felt substrate. The measured result of ARBW in Fig. 11 shows a broadband of 22.03% (5.05–6.3 GHz) compared with the simulated result of 24.17% (5.02–6.4 GHz). The measured gain and radiation efficiency within the ARBW are shown in Fig. 12. The measured broadside gains range from 6.5 to 6.8 dBic. The maximum measured radiation efficiency is 88% at 5.6 GHz. The radiation pattern in free space at 5.85 GHz in two principle x–z and y–z planes is shown in Fig. 13. It can be perceived that the proposed antenna has directional radiation pattern with RHCP in the $+z$ direction. The measured front-to-back ratio (FBR) at 5.85 GHz in the broadside direction is 41 dB. The cross-polarization discrimination at 5.85 GHz is 31 dB.

B. ON-BODY PERFORMANCE

In this section, the proposed antenna is simulated over a $160 \times 160 \times 50$ mm^3 four-layered human tissue. The thickness of the skin, fat, muscle, and bone are 1.5, 8.5, 27.5, and 12.5 mm, respectively, as shown in Fig. 14. The parameters of the relative permittivity and conductivity at 5.85 GHz [30] are listed in Table 1. The antenna is placed 5 mm above the tissue model to approximate the thickness of a garment. The measured S11 on different parts of human body, including on the leg is 43.5% (4.63–7.21 GHz)

Compared with the simulated result of 35.5% (4.76–6.82 GHz) as shown in Fig. 15. The fabricated antenna is mounted on the phantom head for measuring the 3-D radiation pattern in an anechoic chamber, which shows an

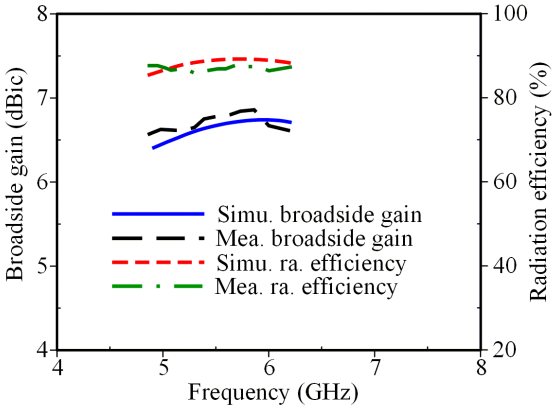

FIGURE 12. Measured broadside gain and radiation efficiency in free space.

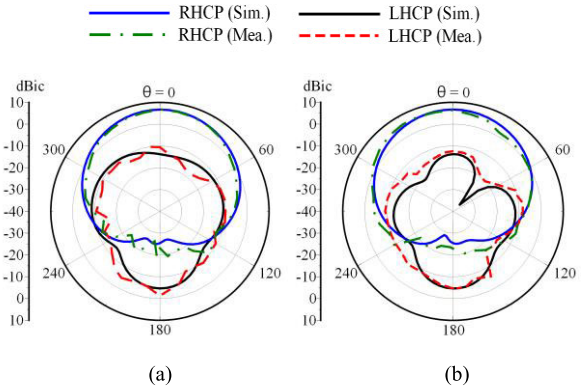

FIGURE 13. Measured radiation pattern at 5.85 GHz in free space: (a) x–z plane and (b) y–z plane.

TABLE 1. Human tissue.

Layer	Permittivity (ϵ_r)	Conductivity (S/m)
Skin	33.8	3.84
Fat	4.2	0.28
Muscle	50	6.48
Bone	15.8	1.77

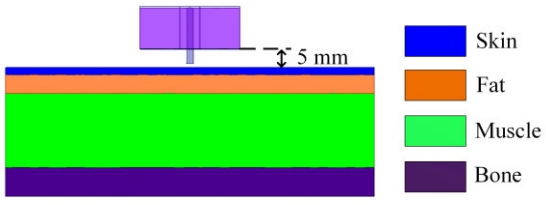

FIGURE 14. Model of four-layered tissue.

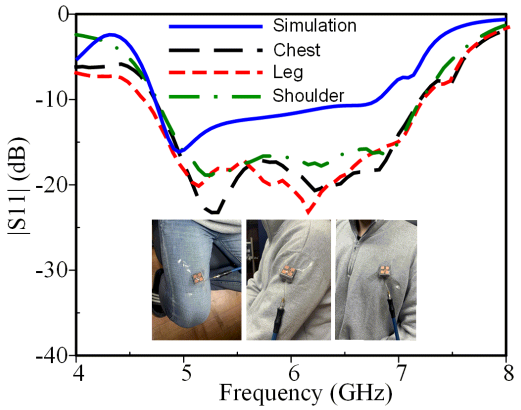

FIGURE 15. Measured S11 results on the human body.

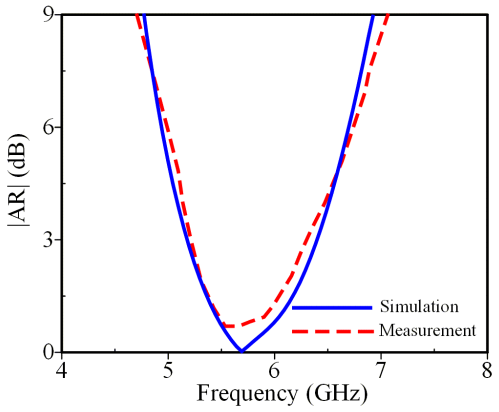

FIGURE 16. Measured AR on a phantom.

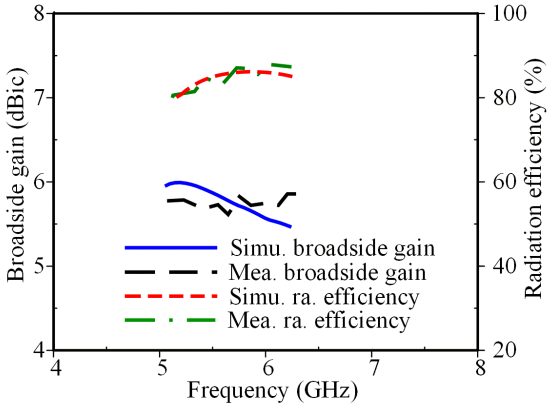

FIGURE 17. Measured broadside gain and radiation efficiency on a phantom.

ARBW of 20.6% (5.18–6.37 GHz) in Fig. 16. The measured broadside gain and radiation efficiency on the phantom head within the ARBW are shown in Fig. 17. The measured broadside gain ranges from 5.4 to 5.8 dBic. The maximum radiation efficiency is 85% at 5.7 GHz.

The simulated and measured radiation patterns in x–z and y–z planes at 5.85 GHz are plotted in Fig. 18. The RHCP is principal polarization in the boresight direction with a cross-polarization discrimination of 30.2 dB. The FBR at this frequency is approximately 56 dB, indicating that it has less radiated energy in the backward direction. The results in the

TABLE 2. Comparison with other wearable CP antennas.

Ref.	IBW (%)	ARBW (%)	Size (λ_0^3)	Gain (dBic)	Efficiency (%)	SAR* (W/kg)
[15]	15.9	2.72	0.41 × 0.41 × 0.045	5.2	79	0.65
[16]	11.8	6.4	1.85 × 1.85 × 0.22	3.5	80	N/A
[17]	3.97	2.93	0.27 × 0.27 × 0.2	2.1	72.6	0.118
[19]**	38.7/109	20.7/98.5	0.17 × 0.20 × 0.006	4.9/3.4	55/74	18.4
Prop.	**40.8**	**22.03**	**0.46 × 0.46 × 0.17**	**6.5**	**88**	**0.6**

* Simulated SAR is normalized with the input power of 500 mW and the US standard for 1g average mass.
** Dual-band antenna

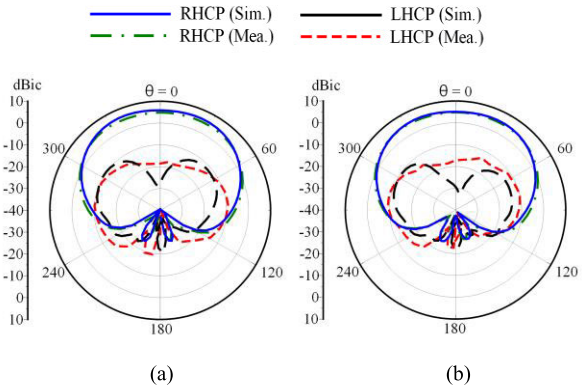

FIGURE 18. Measured radiation pattern at 5.85 GHz on a phantom: (a) x–z plane and (b) y–z plane.

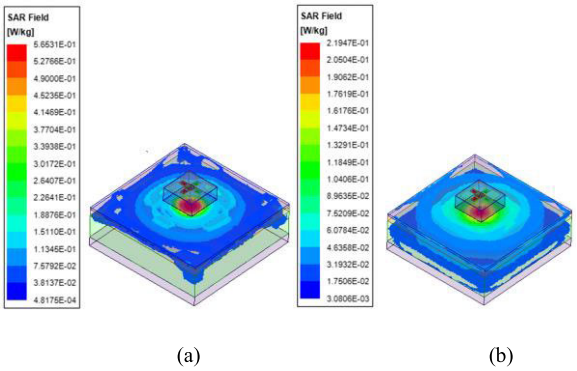

FIGURE 19. Simulated SAR for US and European standards at 5.8 GHz for (a) 1g and (b) 10g tissue, respectively.

phantom body show a slight degradation in broadside gain and radiation efficiency compared with the results in free space because of the proximity effect and the ground plane being bent over the phantom body.

C. SAR EVALUATION

The SAR evaluation is conducted to ensure safe usage by the wearer. The antenna is simulated with an input power of 500 mW. The SAR should be less than the U.S standard of 1.6 W/kg for a 1g average mass and European standard of 2 W/kg for a 10g average mass. As a result, the simulated SARs at 5.85 GHz are 0.57 and 0.22 W/kg for the U.S and European standards, respectively, as shown in Fig. 19, illustrating safe usage on the human body.

The IBW, ARBW, antenna size, broadside gain, radiation efficiency, and SAR of the proposed antenna and other reported CP wearable antennas are summarized in Table 2. In general, the proposed antenna achieves broadband IBW, ARBW, high-gain, and high-efficiency with low SAR.

IV. CONCLUSION

We demonstrated a compact broadband circularly-polarized wearable antenna for WBAN off-body communications. The crossed-dipole antenna loaded with a magneto-electric dipole as the main radiator radiates broadband circularly-polarized waves with high gain and high efficiency. The textile ground plane is attached to the felt substrate, which minimizes the SAR and increases the broadside gain. The fabricated antenna is then verified by measurement in free space and phantom environments, which show good agreement between simulation and measurement. In addition, the simulated SAR ensures the safe usage of the proposed antenna on a human body. The proposed antenna is a potential candidate for WBAN off-body communications.

REFERENCES

[1] K. N. Paracha, S. K. A. Rahim, P. J. Soh, and M. Khalily, "Wearable antennas: A review of materials, structures, and innovative features for autonomous communication and sensing," *IEEE Access*, vol. 7, pp. 56694–56712, 2019.

[2] T. T. Le and T.-Y. Yun, "Miniaturization of a dual-band wearable antenna for WBAN applications," *IEEE Antennas Wireless Propag. Lett.*, vol. 19, no. 8, pp. 1452–1456, Aug. 2020.

[3] T. Le and T.-Y. Yun, "Wearable dual-band high-gain low-SAR antenna for off-body communication," *IEEE Antennas Wireless Propag. Lett.*, vol. 20, no. 7, pp. 1175–1179, Jul. 2021.

[4] A. Smida, A. Iqbal, A. J. Alazemi, M. I. Waly, R. Ghayoula, and S. Kim, "Wideband wearable antenna for biomedical telemetry applications," *IEEE Access*, vol. 8, pp. 15687–15694, 2020.

[5] X. Lin, Y. Chen, Z. Gong, B.-C. Seet, L. Huang, and Y. Lu, "Ultrawideband textile antenna for wearable microwave medical imaging applications," *IEEE Trans. Antennas Propag.*, vol. 68, no. 6, pp. 4238–4249, Jun. 2020.

[6] P. Sambandam, M. Kanagasabai, R. Natarajan, M. G. N. Alsath, and S. Palaniswamy, "Miniaturized button-like WBAN antenna for off-body communication," *IEEE Trans. Antennas Propag.*, vol. 68, no. 7, pp. 5228–5235, Jul. 2020.

[7] A. Y. I. Ashyap, S. H. B. Dahlan, Z. Z. Abidin, M. H. Dahri, H. A. Majid, M. R. Kamarudin, S. K. Yee, M. H. Jamaluddin, A. Alomainy, and Q. H. Abbasi, "Robust and efficient integrated antenna with EBG-DGS enabled wide bandwidth for wearable medical device applications," *IEEE Access*, vol. 8, pp. 56346–56358, 2020.

[8] I. Martinez, C.-X. Mao, D. Vital, H. Shahariar, D. H. Werner, J. S. Jur, and S. Bhardwaj, "Compact, low-profile and robust textile antennas with improved bandwidth for easy garment integration," *IEEE Access*, vol. 8, pp. 77490–77500, 2020.
[9] K. Zhang, G. A. E. Vandenbosch, and S. Yan, "A novel design approach for compact wearable antennas based on metasurfaces," *IEEE Trans. Biomed. Circuits Syst.*, vol. 14, no. 4, pp. 918–927, Aug. 2020.
[10] M. El Gharbi, R. Fernández-García, and I. Gil, "Embroidered wearable antenna-based sensor for real-time breath monitoring," *Measurement*, vol. 195, May 2022, Art. no. 111080.
[11] F. Khajeh-Khalili and Y. Khosravi, "A novel wearable wideband antenna for application in wireless medical communication systems with jeans substrate," *J. Textile Inst.*, vol. 112, no. 8, pp. 1266–1272, Aug. 2021.
[12] F. Khajeh-Khalili, A. Shahriari, and F. Haghshenas, "A simple method to simultaneously increase the gain and bandwidth of wearable antennas for application in medical/communications systems," *Int. J. Microw. Wireless Technol.*, vol. 13, no. 4, pp. 374–380, Aug. 2020.
[13] M. Wagih, A. Komolafe, A. S. Weddell, and S. Beeby, "Broadband compact substrate-independent textile wearable antenna for simultaneous near- and far-field wireless power transmission," *IEEE Open J. Antennas Propag.*, vol. 3, pp. 398–411, 2022.
[14] K. W. Lui, O. H. Murphy, and C. Toumazou, "A wearable wideband circularly polarized textile antenna for effective power transmission on a wirelessly-powered sensor platform," *IEEE Trans. Antennas Propag.*, vol. 61, no. 7, pp. 3873–3876, Jul. 2013.
[15] Z. H. Jiang, Z. Cui, T. Yue, Y. Zhu, and D. H. Werner, "Compact, highly efficient, and fully flexible circularly polarized antenna enabled by silver nanowires for wireless body-area networks," *IEEE Trans. Biomed. Circuits Syst.*, vol. 11, no. 4, pp. 920–932, Aug. 2017.
[16] X. Hu, S. Yan, and G. A. E. Vandenbosch, "Compact circularly polarized wearable button antenna with broadside pattern for U-NII worldwide band applications," *IEEE Trans. Antennas Propag.*, vol. 67, no. 2, pp. 1341–1345, Feb. 2019.
[17] X. Hu, S. Yan, J. Zhang, V. Volski, and G. A. E. Vandenbosch, "Omnidirectional circularly polarized button antenna for 5 GHz WBAN applications," *IEEE Trans. Antennas Propag.*, vol. 69, no. 8, pp. 5054–5059, Aug. 2021.
[18] H. Yang, X. Liu, and Y. Fan, "Design of broadband circularly polarized all-textile antenna and its conformal array for wearable devices," *IEEE Trans. Antennas Propag.*, vol. 70, no. 1, pp. 209–220, Jan. 2022.
[19] M. Kanagasabai, P. Sambandam, M. G. N. Alsath, S. Palaniswamy, A. Ravichandran, and C. Girinathan, "Miniaturized circularly polarized UWB antenna for body centric communication," *IEEE Trans. Antennas Propag.*, vol. 70, no. 1, pp. 189–196, Jan. 2022.
[20] K.-M. Luk and H. Wong, "A new wideband unidirectional antenna element," *Int. J. Microw. Opt. Technol.*, vol. 1, no. 1, pp. 35–44, Jun. 2006.
[21] X. Dai and K. M. Luk, "A wideband dual-polarized antenna for millimeter-wave applications," *IEEE Trans. Antennas Propag.*, vol. 69, no. 4, pp. 2380–2385, Apr. 2021.
[22] S. X. Ta and I. Park, "Crossed dipole loaded with magneto-electric dipole for wideband and wide-beam circularly polarized radiation," *IEEE Antennas Wireless Propag. Lett.*, vol. 14, pp. 358–361, 2015.
[23] Y. Gu, X.-X. Yang, T. Lou, and Y. Wu, "Low-profile dual-band magneto-electric dipole antenna loaded with metasurface," *IEEE Antennas Wireless Propag. Lett.*, vol. 21, no. 7, pp. 1492–1496, Jul. 2022.
[24] S. Trinh-Van, T. Van Trinh, Y. Yang, K.-Y. Lee, and K. C. Hwang, "Bandwidth-enhanced low-profile magneto-electric dipole antenna with shorting parasitic elements," *IEEE Access*, vol. 9, pp. 64852–64859, 2021.
[25] J. Xu, W. Hong, Z. H. Jiang, and H. Zhang, "Low-cost millimeter-wave circularly polarized planar integrated magneto-electric dipole and its arrays with low-profile feeding structures," *IEEE Antennas Wireless Propag. Lett.*, vol. 19, no. 8, pp. 1400–1404, Aug. 2020.
[26] M. Li and K.-M. Luk, "Wideband magneto-electric dipole antenna for 60-GHz millimeter-wave communications," *IEEE Trans. Antennas Propag.*, vol. 63, no. 7, pp. 3276–3279, Jul. 2015.
[27] S. Yan, P. J. Soh, and G. A. E. Vandenbosch, "Wearable dual-band magneto-electric dipole antenna for WBAN/WLAN applications," *IEEE Trans. Antennas Propag.*, vol. 63, no. 9, pp. 4165–4169, Sep. 2015.
[28] T. T. Le, Y.-D. Kim, and T.-Y. Yun, "A triple-band dual-open-ring high-gain high-efficiency antenna for wearable applications," *IEEE Access*, vol. 9, pp. 118435–118442, 2021.
[29] *Shieldit Super Fabric*. Accessed: Aug. 11, 2022. [Online]. Available: http://lessemf.com
[30] *Calculation of the Dielectric Properties of Body Tissues in the Frequency Range 10 Hz–100 GHz*. Accessed: Aug. 11, 2022. [Online]. Available: http://niremf.ifac.cnr.it/tissprop/htmlclie/htmlclie.php

TU TUAN LE received the B.S. degree in electronics and telecommunications from the Hanoi University of Science and Technology, Hanoi, Vietnam, in 2013, and the Ph.D. degree from the Department of Electronics and Electrical Engineering, Dongguk University, Seoul, South Korea. He is currently working as a Research Assistant Professor with Hanyang University, Seoul. His current research interests include RF energy harvesting, wearable antenna, circularly polarized antennas, reconfigurable antennas, and multiband/broadband planar antennas for various wireless applications.

YONG-DEOK KIM received the B.S. degree in information and communication engineering from Hoseo University, South Korea, in 2020. He is currently pursuing the Ph.D. degree with the Department of Electronics Engineering, Hanyang University, Seoul, South Korea. His current research interests include circularly polarized antennas, wearable antennas, multiband antennas, and on-chip antennas for various wireless applications.

TAE-YEOUL YUN (Member, IEEE) received the Ph.D. degree from the Department of Electrical Engineering, Texas A&M University, College Station, TX, USA, in 2001. From 1989 to 1996, he worked with the Optical Telecommunication System Group, ETRI, Daejeon, South Korea, where he developed 2.5- and 10-Gb/s systems. From 2001 to 2003, he was a MMIC Designer at Triquint Semiconductor, Dallas, TX, USA. Since 2003, he has been a Professor with Hanyang University, Seoul, South Korea. His research interests include RFICs, antennas, and wireless/optical high-speed communication systems.